International Journal of Computational Methods

APPLICATION OF POLYGONAL FINITE ELEMENTS IN LINEAR ELASTICITY

A. TABARRAEI

Department of Civil and Environmental Engineering, University of California, Davis, CA 95616, USA.
atabarraei@ucdavis.edu

N. SUKUMAR*

Department of Civil and Environmental Engineering, University of California, Davis, CA 95616, USA.
nsukumar@ucdavis.edu

Received (Day Month Year)
Revised (Day Month Year)

In this paper, a conforming polygonal finite element method is applied to problems in linear elasticity. Meshfree natural neighbor (Laplace) shape functions are used to construct conforming interpolating functions on any convex polygon. This provides greater flexibility to solve partial differential equations on complicated geometries. Closed-form expressions for Laplace shape functions on pentagonal, hexagonal, heptagonal, and octagonal reference elements are derived. Numerical examples are presented to demonstrate the accuracy of the method in two-dimensional elastostatics.

Keywords: barycentric coordinates; meshfree methods; natural neighbors; Laplace interpolant.

1. Introduction

The finite element method is a powerful numerical tool for solving partial differential equations of mathematical physics. The use of triangular and quadrilateral elements are well-established in conventional finite element methods. However, there is significant bottleneck in generating quality meshes using three- and four-sided elements for complex geometries. The use of elements with a large number of sides will provide greater flexibility and better accuracy to solve problems that arise in solid mechanics and biomechanics. Since material microstructure in polycrystalline alloys and piezoelectrics, and bone can be described through polygonal sub-domains, the use of polygonal finite elements in such applications is a natural choice. Wachspress [Wachspress (1975)] proposed the construction of basis functions on convex

*Corresponding author. Department of Civil and Environmental Engineering, University of California, One Shields Avenue, Davis, CA 95616, USA.

polygons (n-gons) with any number of sides. Wachspress's rational basis functions are defined as polynomials of $n-2$ divided by polynomials of $n-3$. Recently, significant advances have been achieved in the construction of barycentric coordinates on irregular polygons [Meyer *et al.* (2002); Dasgupta (2003); Floater (2003); Malsch and Dasgupta (2004); Sukumar and Tabarraei (2004)]. A simplified expression for Wachspress basis functions is presented by Meyer *et al.* [2002], and Floater [2003] derived barycentric coordinates in which a vertex in a planar triangulation is expressed as a convex combination of its neighboring vertices. In Sukumar and Tabarraei [2004], natural neighbor (Laplace) interpolation [Christ *et al.* (1982)] is used to construct $C^0(\Omega)$ shape functions on polygonal elements and this procedure has been used for h-adaptive refinement on quadtree meshes [Tabarraei and Sukumar (2005)]. The construction of polygonal approximants using the principle of maximum entropy is described in Sukumar [2004].

In this paper, Laplace interpolants are constructed on reference polygonal elements, and through an isoparametric map, shape functions on physical elements are constructed. As shown in Sukumar *et al.* [2001], Laplace interpolants are linear on element boundaries and can exactly reproduce constant and linear fields. This permits the direct imposition of essential boundary conditions in polygonal finite elements [Sukumar and Tabarraei (2004)]. The outline of this paper is as follows. The construction of Laplace interpolant on irregular convex polygons is presented in Section 2. The model problem is described in Section 3, and numerical examples (patch test, beam bending, edge crack) are presented in Section 4. Finally, some concluding remarks are mentioned in Section 5.

2. Conforming Polygonal Shape Functions

In this section, we review the construction of conforming interpolants on irregular polygons. The interested reader can see Sukumar and Tabarraei [2004] for a detailed description of the method. Consider a domain Ω that is discretized by a set of nodes. If a point p is inserted inside the domain, the Voronoi cell of point p is the locus of all points that are closer to p than to any other node inside the domain. The Delaunay tessellation can be obtained by connecting those nodes that have a common edge. The Voronoi cells, Delaunay triangles and Delaunay circumcircles are shown in Fig. 1. If the point p lies inside the circumcircle of a Delaunay triangulation, all those nodes that form the Delaunay triangle are considered as the natural neighbors of point p [Sibson (1980)]. For example in Fig. 1b, nodes 1, 2, 5 and 6 are natural neighbors of p.

As in classical finite elements, to construct an interpolant on the physical element, first the interpolant is defined on a reference element. Polygonal reference elements (pentagon, hexagon, heptagon, and octagon) in the $\boldsymbol{\xi}$-coordinate system are depicted in Fig. 2. From Fig. 2, we observe that all vertex nodes lie on the circumcircle of the reference element. This property ensures that all the nodes of the reference element are natural neighbors of any point within the polygon. Referring

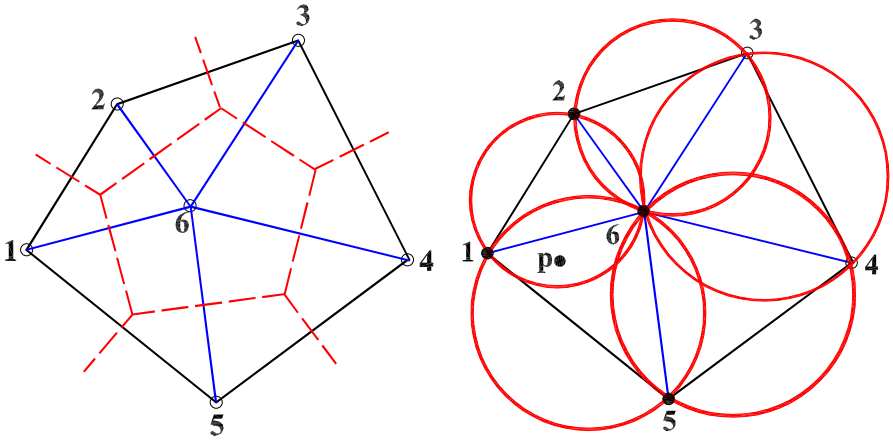

Fig. 1. (a)Voronoi cells and Delaunay triangles; and (b) Delaunay triangles and Delaunay circumcircles.

to Fig. 3, the Laplace shape functions at point p are defined as

$$\phi_i(\boldsymbol{\xi}) = \frac{\alpha_i(\boldsymbol{\xi})}{\sum_{j=1}^{n} \alpha_j(\boldsymbol{\xi})}, \quad \alpha_j(\boldsymbol{\xi}) = \frac{s_j(\boldsymbol{\xi})}{h_j(\boldsymbol{\xi})}, \quad \boldsymbol{\xi} \in \Omega_0, \tag{1}$$

where $\alpha_i(\boldsymbol{\xi})$ is the Laplace weight function, $s_i(\boldsymbol{\xi})$ is the length of the common edge between Voronoi cell of point p and node i, and $h_i(\boldsymbol{\xi})$ is the Euclidean distance between point p and node i. The Laplace shape functions satisfy the following properties [Christ *et al.* (1982)]:

(1) Non-negative, interpolate, and form a partition of unity:

$$0 \leq \phi_i(\boldsymbol{\xi}) \leq 1, \quad \phi_i(\boldsymbol{\xi}_j) = \delta_{ij}, \quad \sum_{i=1}^{n} \phi_i(\boldsymbol{\xi}) = 1, \tag{2}$$

where δ_{ij} is the Kronecker-delta.

(2) Linear completeness [Hughes (1987)]:

$$\mathbf{x}(\boldsymbol{\xi}) = \sum_{i=1}^{n} \phi_i(\boldsymbol{\xi}) \mathbf{x}_i, \tag{3}$$

which in conjunction with Eq. (2) implies that the Laplace interpolant can exactly reproduce arbitrary constant and linear functions.

To obtain the polygonal shape functions and their derivatives on the physical element, we use the isoparametric transformation given in Eq. (3). Since the Laplace interpolant is linear on any edge of the reference element (only two shape functions are non-zero), the isoparametric mapping preserves this property on the physical

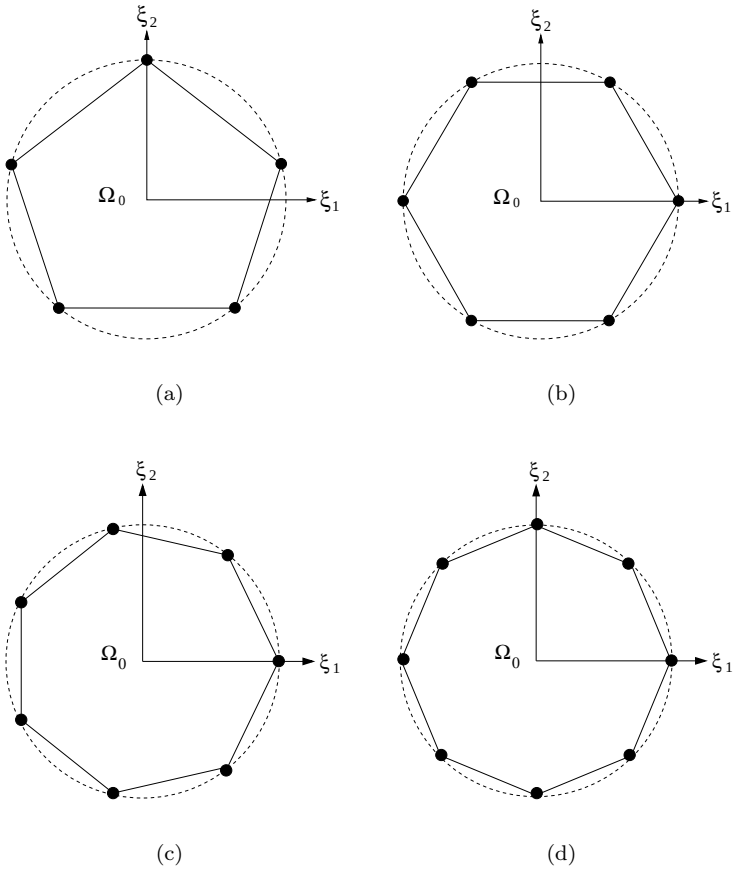

Fig. 2. Reference elements. (a) Pentagon; (b) Hexagon; (c) Heptagon; and (d) Octagon.

element, which leads to $C^0(\Omega)$ conformity of the interpolant (Fig. 4). It was shown in Sukumar *et al.* [2001] that Laplace shape functions are identical to barycentric (area coordinates) shape functions on the triangle and to bilinear finite element shape functions on the bi-unit square. Hence, the extension of existing finite element programs to polygonal finite element codes is straightforward.

The Laplace interpolant reproduces Wachspress interpolant on regular polygons, and the Laplace weight function, $\alpha_i(\boldsymbol{\xi})$, at any point inside the reference element is given by [Sukumar and Tabarraei (2004)]:

$$\alpha_i(\boldsymbol{\xi}) = \frac{2(1-\xi_1^2-\xi_2^2)\sin^3\frac{\pi}{n}\cos\frac{\pi}{n}}{A_{i-1}A_i}. \tag{4}$$

In the above equation, A_i is the area of the triangle $[p, p_i, p_{i+1}]$ and A_{i-1} is the area of triangle $[p, p_{i-1}, p_i]$ (Fig. 5). On using Eq. (4), closed-form expressions for shape

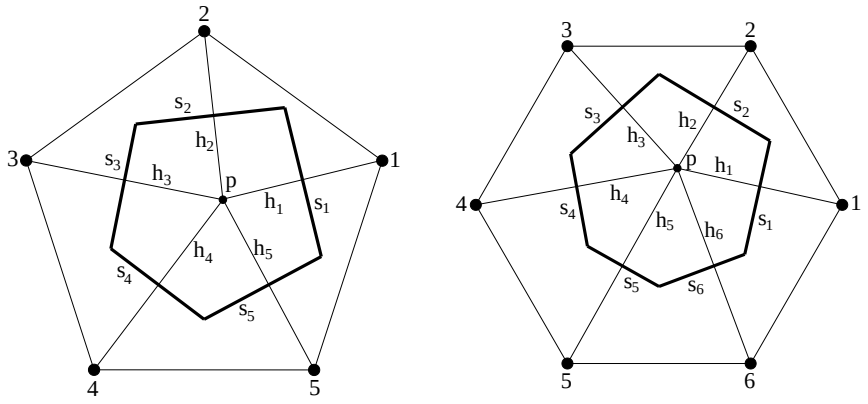

(a) (b)

Fig. 3. Voronoi cell of point p and construction of Laplace shape function. (a) Pentagonal reference element; and (b) Hexagonal reference element.

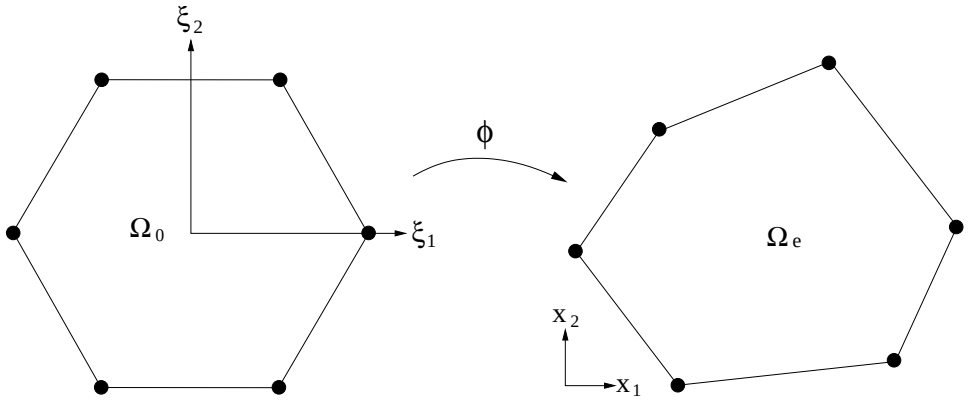

Fig. 4. Isoparametric mapping.

functions on regular n-gons can be obtained by employing a symbolic program such as *Mathematica*$^{\text{TM}}$. The shape functions for a regular pentagon, hexagon, heptagon, and octagon are presented in the Appendix.

Extension of numerical quadrature rules from triangular and quadrilateral elements to convex polygons with more than four edges is a non-trivial task. No general quadrature rule is available for the purpose of integrating functions (polynomial or rational) on polygonal domains. In this paper, the Gaussian quadrature rule for triangular elements is used to evaluate weak form integrals on polygonal elements. For the purpose of numerical integration, the polygonal reference element is partitioned

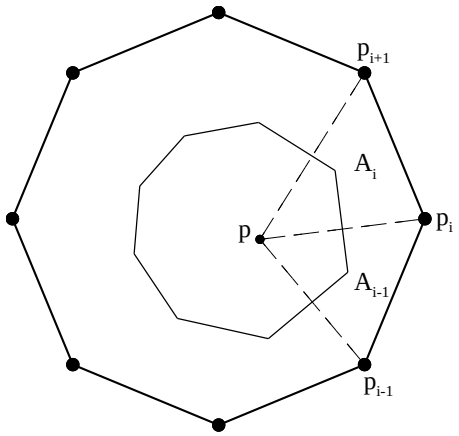

Fig. 5. Equivalence of Laplace and Wachspress shape functions on a regular n-gon ($n = 8$).

into n isosceles sub-triangles. An affine map is used from the triangular reference element to the sub-triangle of the polygonal reference element to find the location of Gauss points inside the reference element. To find the location of the Gauss points in the physical element, the isoparametric map from the reference element to the physical element is used. The contributions from each sub-triangle are added up to obtain the integral value over the polygonal element. This procedure is illustrated in Fig. 6 and can be expressed as [Sukumar and Tabarraei (2004)]

$$\int_{\Omega_e} f\, d\Omega = \int_{\Omega_0} f\, |\mathbf{J}_2| d\Omega = \sum_{j=1}^{n} \int_{\Omega_0^{\triangle_j}} f\, |\mathbf{J}_2| d\Omega = \sum_{j=1}^{n} \int_0^1 \int_0^{1-\xi} f |\mathbf{J}_1^j| |\mathbf{J}_2|\, d\xi d\eta. \tag{5}$$

3. Governing Equations and Weak Form in Linear Elasticity

The equilibrium equation of linear elastostatics in the absence of body forces is:

$$\nabla \cdot \boldsymbol{\sigma} = 0 \quad \text{in } \Omega \tag{6}$$

with boundary conditions

$$\mathbf{u} = \bar{\mathbf{u}} \quad \text{on } \Gamma_u \text{ (displacement boundary)} \tag{7a}$$

$$\boldsymbol{\sigma} \cdot \mathbf{n} = \bar{\mathbf{t}} \quad \text{on } \Gamma_t \text{ (traction boundary)} \tag{7b}$$

where $\Gamma = \Gamma_t \cup \Gamma_u$ and $\Gamma_u \cap \Gamma_t = \emptyset$. In Eq. (7), $\mathbf{u}$ is the displacement vector and $\boldsymbol{\sigma}$ is the stress tensor.

In the finite element method, displacements are approximated by

$$\mathbf{u}^h = \sum_i N_i u_i = \mathbf{N}\mathbf{u}, \tag{8}$$

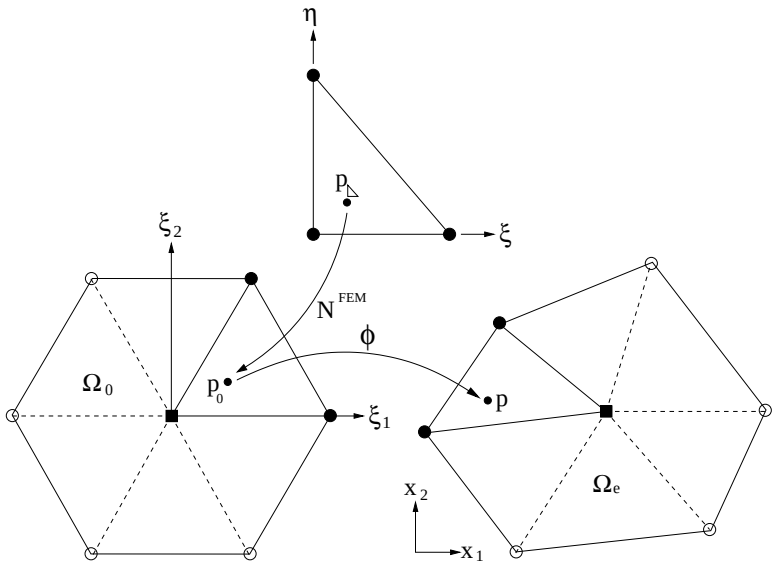

Fig. 6. Numerical integration scheme based on the partition of the canonical element.

where N_i is the finite element shape function for node i and u_i is the displacement at the ith node. The finite element approximation for the strain tensor is defined as

$$\boldsymbol{\varepsilon} = \mathbf{B}\mathbf{u}, \tag{9}$$

where $\mathbf{B}$ is the element strain-displacement operator. Using the constitutive law, the stress matrix can be defined as

$$\boldsymbol{\sigma} = \mathbf{D}\boldsymbol{\varepsilon} = (\mathbf{D}\mathbf{B})\mathbf{u}, \tag{10}$$

where $\mathbf{D}$ is the constitutive matrix. The variational form (principle of virtual work) of the equilibrium equation is:

$$\int_{\Omega} \delta\boldsymbol{\varepsilon}^T \boldsymbol{\sigma} - \int_{\Gamma_t} \delta\mathbf{u}^T \bar{\mathbf{t}} d\Gamma = 0 \quad \forall \delta u_i \in H_0^1(\Omega), \tag{11}$$

where δ denotes the variation operator, and $H_0^1(\Omega)$ is the Sobolev space of functions with square-integrable derivatives up to order one and vanishing value on Γ_u. On using a standard Galerkin procedure, we obtain the discrete equations:

$$\mathbf{K}\mathbf{u} = \mathbf{f}, \tag{12a}$$

$$\mathbf{K} = \int_{\Omega} \mathbf{B}^T \mathbf{D}\mathbf{B} d\Omega, \tag{12b}$$

$$\mathbf{f} = \int_{\Gamma_t} \mathbf{N}^T \bar{\mathbf{t}} d\Gamma. \tag{12c}$$

For an isotropic material in plane stress condition, the stress-strain relationship is defined as

$$\begin{bmatrix} \sigma_x \\ \sigma_y \\ \sigma_{xy} \end{bmatrix} = \frac{E}{1-\nu^2} \begin{bmatrix} 1 & \nu & 0 \\ \nu & 1 & 0 \\ 0 & 0 & \dfrac{1-\nu}{2} \end{bmatrix} \begin{bmatrix} \varepsilon_x \\ \varepsilon_y \\ \varepsilon_{xy} \end{bmatrix}, \tag{13}$$

where ν is the Poisson's ratio and E is the Young's modulus. The constitutive equations of plane strain case can be obtained from plane stress equations by replacing E by $\dfrac{E}{1-\nu^2}$ and ν by $\dfrac{\nu}{1-\nu}$.

4. Numerical Results

We present four examples to assess the performance of the polygonal finite element method. For the purpose of error estimation and convergence studies, the L^2 norm and energy norm of the displacement error are employed. In our analyses, the L^2 norm and energy norm of the displacement error are defined as

$$||\mathbf{u}-\mathbf{u}^h||_{L^2} = \left(\int_\Omega \left[(\mathbf{u}-\mathbf{u}^h)\cdot(\mathbf{u}-\mathbf{u}^h) \right] d\Omega \right)^{\frac{1}{2}}, \tag{14a}$$

$$\|\mathbf{u}-\mathbf{u}^h\|_{E(\Omega)} = \sqrt{a(\mathbf{u}-\mathbf{u}^h, \mathbf{u}-\mathbf{u}^h)}, \quad a(\mathbf{u},\mathbf{u}) = \int_\Omega \boldsymbol{\varepsilon}^T \mathbf{D} \boldsymbol{\varepsilon}\, dV, \tag{14b}$$

where $\mathbf{u}$ and $\mathbf{u}^h$ are the exact and numerical solutions, respectively.

To perform numerical integration on n-gons with $n > 4$, the procedure described in Section 2 is employed with 25 Gauss points in each sub-triangle. On three-noded triangular elements, one point quadrature is adopted and on four-noded bilinear elements, 2×2 Gauss-Legendre quadrature rule is used.

4.1. *Displacement patch test*

First, the ability of polygonal finite elements to represent linear displacement fields is studied. The domain is the unit square and two different sets of boundary conditions are considered. For the first test, $\mathbf{u} = x_1 + x_2$ is applied on the boundary of the domain; the second test is performed by applying $u_1 = x_2$ and $\mathrm{u}_2 = \mathrm{x}_1$ on the boundary of the domain. In Fig. 7, three different meshes that are considered in this analysis are shown. The L^2 norm and energy norm of displacement error is shown in Table 1, and the results reveal that the patch test is passed to $\mathcal{O}(10^{-8})$ and $\mathcal{O}(10^{-7})$ accuracy in L^2 and energy norm, respectively.

4.2. *Equilibrium patch test*

The ability to represent a uniaxial plane stress field is verified by the equilibrium patch test. Consider a uniaxial stress $\sigma = 1$ psi (plane stress conditions are assumed)

Table 1. Relative error in the L^2 norm and energy norm for the displacement patch test.

Meshes	Number of nodes	Relative error in the L^2 norm		Relative error in the energy norm	
		$u_1 = x_1 + x_2$ $u_2 = x_1 + x_2$	$u_1 = x_2$ $u_2 = x_1$	$u_1 = x_1 + x_2$ $u_2 = x_1 + x_2$	$u_1 = x_2$ $u_2 = x_1$
a	22	3.53×10^{-10}	3.40×10^{-10}	2.64×10^{-9}	1.85×10^{-9}
b	102	2.17×10^{-9}	1.49×10^{-9}	4.29×10^{-8}	2.97×10^{-8}
c	1002	3.45×10^{-9}	3.04×10^{-9}	1.50×10^{-7}	1.14×10^{-7}
d	1521	1.11×10^{-9}	9.49×10^{-10}	7.72×10^{-8}	5.63×10^{-8}

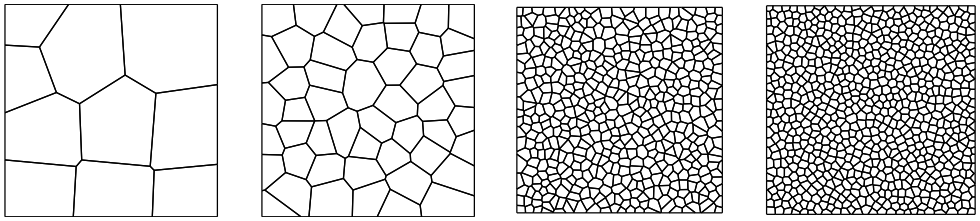

(a) (b) (c) (d)

Fig. 7. Patch test on polygonal meshes. (a) Mesh *a* (22 nodes); (b) Mesh *b* (102 nodes); (c) Mesh *c* (1001 nodes) and (d) Mesh *d* (1521 nodes).

in the x_2-direction acting on the top edge of the unit square shown in (Fig. 8). The displacement of the bottom edge is fixed in the x_2 direction. The essential boundary conditions are indicated in Fig. 8. The exact displacement solution is [Sukumar *et al.* (1998)]:

$$u_1(x_1, x_2) = \frac{\nu}{E}(1 - x_1), \tag{15a}$$

$$u_2(x_1, x_2) = \frac{x_2}{E}. \tag{15b}$$

The meshes shown in Fig. 7 are considered in the analyses. The relative error in the L^2 norm and the energy norm are presented in Table 2. Relative errors of $\mathcal{O}(10^{-5})$ in L^2 norm and energy norm are obtained for this problem.

4.3. *Cantilever beam*

In Fig. 9, a cantilever beam subjected to a parabolic end load is illustrated. The beam has length L, height D, and unit width. The top and bottom edges of the beam are traction free. The left edge is fixed in the x_1 and x_2 direction. The displacement

Table 2. Relative error in the L^2 norm and energy norm for the equilibrium patch test.

Meshes	Number of Nodes	Relative error in the L^2 norm	Relative error in the energy norm
a	22	2.22×10^{-6}	3.11×10^{-6}
b	102	4.77×10^{-6}	3.68×10^{-6}
c	1002	9.25×10^{-6}	6.44×10^{-6}
d	1521	9.59×10^{-6}	7.07×10^{-6}

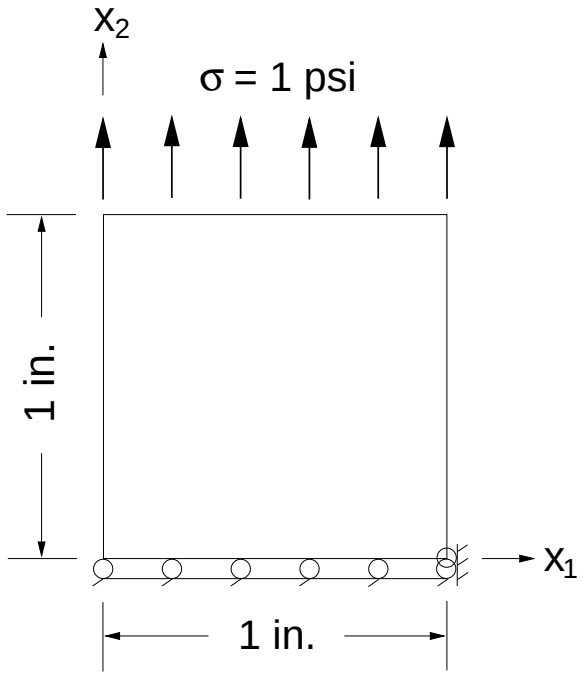

Fig. 8. Equilibrium (uniaxial tension) patch test [Sukumar *et al.* (1998)].

vector solution is given by [Timoshenko and Goodier (1987)]

$$u_1(x_1, x_2) = \frac{-Px_2}{6\bar{E}I}\left[(6L - 3x_1)x_1 + (2 + \bar{\nu})\left(x_2^2 - \frac{D^2}{4}\right)\right], \tag{16a}$$

$$u_2(x_1, x_2) = \frac{P}{6\bar{E}I}\left[3\bar{\nu}x_2^2(L - x_1) + (4 + 5\bar{\nu})\frac{D^2 x_1}{4} + (3L - x_1)x_1^2\right], \tag{16b}$$

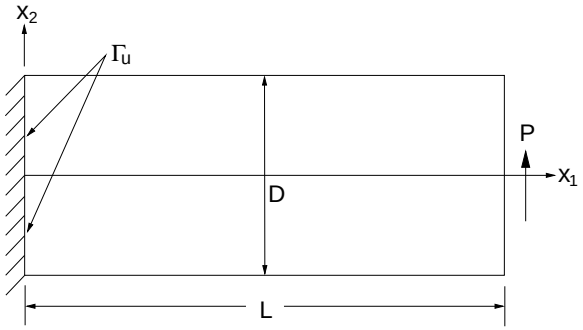

Fig. 9. Cantilever beam model [Sukumar *et al.* (1998)].

where

$$\bar{E} = \begin{cases} E & \text{(plane stress)}, \\ \dfrac{E}{1-\nu^2} & \text{(plane strain)}, \end{cases} \tag{17a}$$

$$\bar{\nu} = \begin{cases} \nu & \text{(plane stress)}, \\ \dfrac{\nu}{1-\nu} & \text{(plane strain)}. \end{cases} \tag{17b}$$

The stresses are given by

$$\sigma_{11}(x_1, x_2) = \frac{-P(L-x_1)x_2}{I}, \tag{18a}$$

$$\sigma_{22}(x_1, x_2) = 0, \tag{18b}$$

$$\sigma_{12}(x_1, x_2) = \frac{P}{2I}\left(\frac{D^2}{4} - x_2^2\right), \tag{18c}$$

where I is the moment of inertia, which for a beam with rectangular cross-section and unit thickness is:

$$I = \frac{D^3}{12}. \tag{18d}$$

In the finite element computations, the following parameters are used: $P = -1000$ lb, $D = 1$ in., $L = 8$ in., $E = 2 \times 10^5$ psi, $\nu = 0.3$ and plane strain conditions are assumed. To compare the results, we use quadrilateral and polygonal meshes to solve the problems. The polygonal meshes are shown in Fig. 10. The quadrilateral meshes are composed of 180 (30×6) and 1890 (105×18) elements. The exact end deflection $u_2(L, 0) = 9.430$ in. In Tables 3 and 4, the numerically computed end deflection is compared with that obtained from engineering beam theory. The numerical results using polygonal meshes are in good agreement with beam theory predictions.

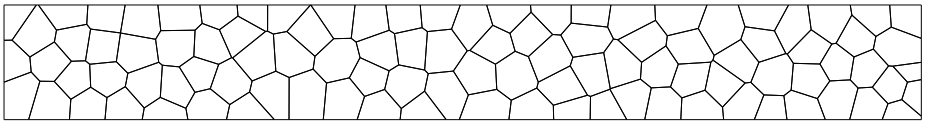

(a)

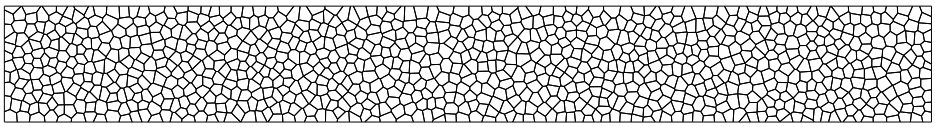

(b)

Fig. 10. Polygonal meshes of cantilever beam. (a) Mesh *a* (202 nodes); and (b) Mesh *b* (2001 nodes).

4.4. *Stress intensity factor computations for an edge crack*

Stress intensity factor (SIF) computations for an edge cracked specimen are presented. To compute the stress intensity factors, the domain form of the interaction integral is used [Yau *et al.* (1980); Moran and Shih (1987)]. Two sets of boundary conditions are considered. As the first problem, a crack of length a in a semi-infinite elastic plate subjected to uniform loading is considered. The loading can be decom-

Table 3. Deflection of the cantilever beam using polygonal elements.

Meshes	Number of elements	Number of nodes	Normalized end deflection
a	100	202	0.94
b	1000	2001	0.99

Table 4. Deflection of the cantilever beam using quadrilateral elements.

Meshes	Number of elements	Number of nodes	Normalized end deflection
a	180	217	0.97
b	1890	2014	0.99

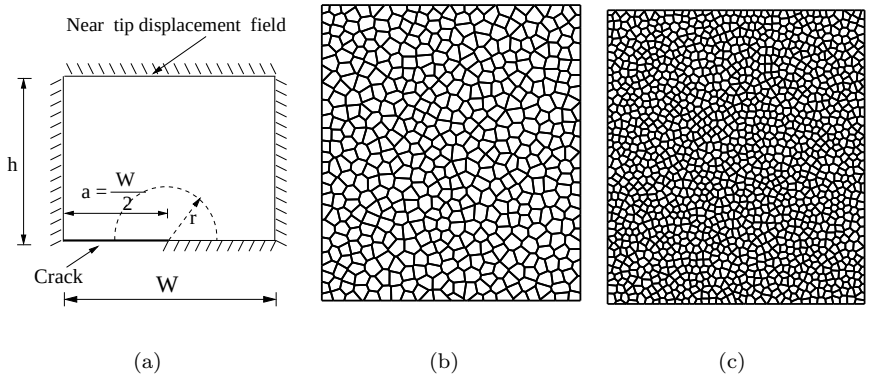

Fig. 11. The semi-infinite edge crack problem. (a) Interaction integral domain and boundary conditions; (b) Mesh *a* (1002 nodes); and (c) Mesh *b* (2895 nodes).

posed into an opening (K_I) and a shearing mode (K_{II}). To calculate the stress intensity factors, a small region near the crack tip is considered. The exact near-tip displacement field is imposed on the boundary, with $K_I = 1$ and $K_{II} = 1$. To verify the domain independence of the computations, the SIFs are evaluated for three different contours. The contour interaction integral domains and the boundary conditions are shown in Fig. 11a, and polygonal discretization of the domains are shown in Fig. 11b and *c*. The problem parameters are: $W = 7.0$ in. and $h = 8.0$ in.. The numerical results of stress intensity factors are shown in Table 5. The SIF results are domain independent and accurate. For the second problem, a finite-dimensional plate subjected to uniform tension on the top surface under plane stress is considered. The geometry and boundary conditions of the problem are shown in Fig. 12. The following parameter are chosen: $W = 7.0$ in. and $h = 16.0$ in.. Due to symmetry, half of the domain is analyzed. For the boundary conditions shown in Fig. 12, the exact normalized stress intensity factor $\dfrac{K_{\mathrm{I}}^{\mathrm{ref}}}{\sigma\sqrt{\pi a}} = 2.8264$ [Tada *et al.* (2000)]. The polygonal meshes of Fig. 11 are used in this analysis, and the computed stress intensity factors are presented in Table 6. The numerical results are within two percent of the reference solution.

5. Conclusions

In this paper, we reviewed the construction of Laplace shape functions on irregular convex polygons. We showed that the Laplace interpolant is a generalization of three- and four-noded element to convex polygons with any number of vertices. Due to the appealing properties of the Laplace interpolant, the extension of classical finite element codes to polygonal finite elements is simple and direct. Closed-form expressions for shape functions on pentagonal, hexagonal, heptagonal, and octag-

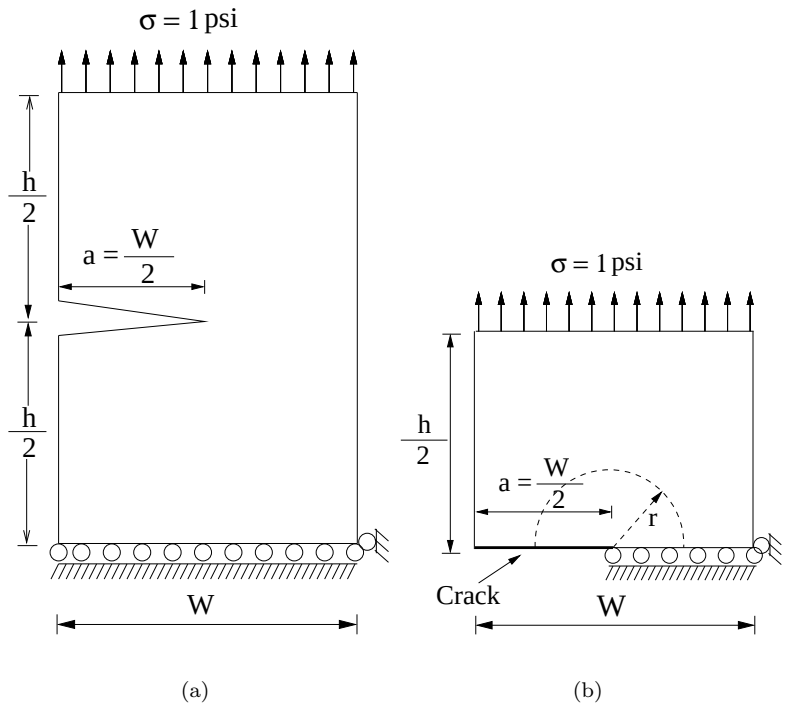

Fig. 12. The finite dimensional edge crack problem. (a) Domain and boundary conditions; and (b) Interaction integral domain and model used in the numerical computations.

onal reference elements were presented. In the numerical integration of the weak form, a higher-order Gaussian quadrature rule was used. The polygonal finite element method passed the displacement patch test to $\mathcal{O}(10^{-8})$ in the L^2 norm and $\mathcal{O}(10^{-7})$ in energy norm. Error in the L^2 norm and energy norm of $\mathcal{O}(10^{-5})$ was obtained for the equilibrium patch test. Machine precision accuracy is not realized in the patch test computations due to the errors introduced in the numerical integration of the weak form integrals. Accurate numerical results for the cantilever

Table 5. Normalized SIF: Semi-infinite edge crack problem.

	Mesh a		Mesh b	
r	K_I	K_{II}	K_I	K_{II}
0.2a	0.9845	1.0366	0.9885	1.0171
0.3a	0.9915	1.0321	0.9925	1.0164
0.5a	0.9949	1.0158	0.9956	1.0156

beam and edge cracked plate problems were obtained.

6. Acknowledgments

The financial support of this work by the National Science Foundation through research award CMS-0352654 to the University of California, Davis, is gratefully acknowledged.

References

Christ, N. H., Friedberg, R. and Lee, T. D. (1982). Weights of links and plaquettes in a random lattice. *Nuclear Physics B.*, **210**: 337–346.

Dasgupta, G. (2003). Interpolants within convex polygons: Wachspress' shape functions. *Journal of Aerospace Engineering*, **16**: 1–8.

Floater, M. S. (2003). Mean value coordinates. *Computer Aided Geometric Design*, **20**: 19–27.

Hughes, T. J. R. (1987). *The Finite Element Method*, Prentice-Hall, Prentice-Hall.

Malsch, E. A. and Dasgupta, G. (2004). Interpolations for temperature distributions: A method for all non-concave polygons. *International Journal of Solids and Structures*, **41**: 2165–2188.

Meyer, M., Lee H., Barr, A. H. and Desbrun, M. (2002). Generalized barycentric coordinates for irregular polygons. *Journal of Graphics Tools*, **7**: 13–22.

Moran, B. and Shih, C. F. (1987). Crack tip and associated domain integrals from momentum and energy balance. *Engineering Fracture Mechanics*, **27**: 615–642.

Sibson, R. (1980). A vector identity for the Dirichlet tesselation. *Mathematical Proceedings of the Cambridge Philosophical Society*, **87**: 151–155.

Sukumar, N., Moran, B., Semenov, A. Yu and Belikov, V. V. (2001). Natural neighbor Galerkin methods. *International Journal for Numerical Methods in Engineering*, **50**: 1–27.

Sukumar, N. (2004). Construction of polygonal interpolants: A maximum entropy approach. *International Journal for Numerical Methods in Engineering*, **12**: 2159–2181.

Sukumar, N., Moran, B. and Belytschko, T. (1998). The natural element method in solid mechanics. *International Journal for Numerical Methods in Engineering*, **43**: 839–887.

Sukumar, N. and Tabarraei, A. (2004). Conforming polygonal finite elements. *International Journal for Numerical Methods in Engineering*, **61**: 2045–2066.

Tabarraei, A. and Sukumar, N. (2005). Adaptive computations on conforming quadtree meshes. *Finite elements in Analysis and Design*, **41**: 686–702.

Table 6. Normalized SIF: Finite-dimensional edge cracked plate under tension.

r	Mesh a		Mesh b	
	$\left(\frac{K_{\mathrm{I}}^{\mathrm{ref}}}{\sigma\sqrt{\pi a}}\right)$	%Error	$\left(\frac{K_{\mathrm{I}}^{\mathrm{ref}}}{\sigma\sqrt{\pi a}}\right)$	%Error
$0.1a$	2.7347	3.2	2.7357	3.2
$0.2a$	2.7704	1.9	2.7721	1.9
$0.3a$	2.7705	1.9	2.7724	1.9

Tada H., Paris, P. C. and Irwin, G. R. (2000). *The Stress Analysis of Cracks Handbook*, ASME Press, New York, N.Y.

Timoshenko, S. P. and Goodier, J. N. (1987). *Theory of Elasticity*, McGraw-Hill, New York, N.Y.

Wachspress, E. L. (1975). *A Rational Finite Element Basis*, Academic Press, New York.

Yau J. , Wang, S. and Corten, H. (1980). A mixed-mode crack analysis of isotropic solids using conservation laws of elasticity. *Journal of Applied Mechanics*, **47**: 335-341.

Appendix A. Appendices

Shape functions on regular convex n-gons are derived. The nodal coordinates of a regular n-gon are:

$$\xi_1^m = \cos\frac{2\pi m}{n}, \quad \xi_2^m = \sin\frac{2\pi m}{n} \quad (\mathrm{m} = 1, 2, \ldots, \mathrm{n}).$$

A.1. *Pentagonal reference element (n = 5)*

$$N_i(\boldsymbol{\xi}) = \frac{a_i(\boldsymbol{\xi})}{b(\boldsymbol{\xi})} \quad (\mathrm{i} = 1, 2, \ldots, 5),$$

where

$$b(\boldsymbol{\xi}) = 87.05 - 12.7004\,\xi_1^2 - 12.7004\,\xi_2^2,$$

and

$$\begin{aligned}
a_1(\boldsymbol{\xi}) =& -0.092937\,(3.23607 + 4\xi_1) \\
&(-3.80423 + 3.80423\xi_1 - 2.76393\xi_2)\,(15.2169 + 5.81234\xi_1 + 17.8885\xi_2)\,, \\
a_2(\boldsymbol{\xi}) =& -0.0790569\,(3.80423 - 3.80423\xi_1 - 2.76393\xi_2) \\
&(-3.80423 + 3.80423\xi_1 - 2.76393\xi_2)\,(15.2169 + 5.81234\xi_1 + 17.8885\xi_2)\,, \\
a_3(\boldsymbol{\xi}) =& -0.0790569\,(15.2169 + 5.81234\xi_1 - 17.8885\xi_2) \\
&(3.80423 - 3.80423\xi_1 - 2.76393\xi_2)\,(-3.80423 + 3.80423\xi_1 - 2.76393\xi_2)\,, \\
a_4(\boldsymbol{\xi}) =& 0.092937\,(3.23607 + 4.\xi_1) \\
&(15.2169 + 5.81234\xi_1 - 17.8885\xi_2)\,(3.80423 - 3.80423\xi_1 - 2.76393\xi_2)\,, \\
a_5(\boldsymbol{\xi}) =& 0.0232343\,(3.23607 + 4.\xi_1) \\
&(15.2169 + 5.81234\xi_1 - 17.8885\xi_2)\,(15.2169 + 5.81234\xi_1 + 17.8885\xi_2)\,.
\end{aligned}$$

A.2. *Hexagonal reference element (n = 6)*

$$
\begin{aligned}
N_1(\boldsymbol{\xi}) &= \frac{\left(\sqrt{3}\xi_1 - \xi_2 - \sqrt{3}\right)\left(2\xi_2 + \sqrt{3}\right)\left(3\,\xi_1^2 + 6\xi_1 - \xi_2^2 + 3\right)}{18\,(\xi_1^2 + \xi_2^2 - 3)},\\
N_2(\boldsymbol{\xi}) &= -\frac{\left(\sqrt{3}\xi_1 + \xi_2 + \sqrt{3}\right)\left(2\xi_2 + \sqrt{3}\right)\left(3\,\xi_1^2 - 6\xi_1 - \xi_2^2 + 3\right)}{18\,(\xi_1^2 + \xi_2^2 - 3)},\\
N_3(\boldsymbol{\xi}) &= \frac{\left(3\xi_1^2 - 6\xi_1 - \xi_2^2 + 3\right)\left(4\xi_2^2 - 3\right)}{18\;(\xi_1^2 + \xi_2^2 - 3)},\\
N_4(\boldsymbol{\xi}) &= -\frac{\left(\sqrt{3} - 2\xi_2\right)\left(\sqrt{3}\xi_1 - \xi_2 + \sqrt{3}\right)\left(3\,\xi_1^2 - 6\xi_1 - \xi_2^2 + 3\right)}{18\,(\xi_1^2 + \xi_2^2 - 3)},\\
N_5(\boldsymbol{\xi}) &= \frac{\left(\sqrt{3} - 2\xi_2\right)\left(\sqrt{3}\xi_1 + \xi_2 - \sqrt{3}\right)\left(3\,\xi_1^2 + 6\xi_1 - \xi_2^2 + 3\right)}{18\,(\xi_1^2 + \xi_2^2 - 3)},\\
N_6(\boldsymbol{\xi}) &= \frac{\left(3\xi_1^2 + 6\xi_1 - \xi_2^2 + 3\right)\left(4\xi_2^2 - 3\right)}{18\;(\xi_1^2 + \xi_2^2 - 3)}.
\end{aligned}
$$

A.3. *Heptagonal reference element (n = 7)*

$$
\begin{aligned}
N_1(\boldsymbol{\xi}) &= \frac{1}{(-0.781831 + 0.781831\xi_1 + 0.37651\xi_2)(0.781831 - 0.193096\xi_1 - 0.846011\xi_2)H},\\
N_2(\boldsymbol{\xi}) &= \frac{1}{(0.781831 + 0.541044\xi_1 - 0.678448\xi_2)(-0.781831 + 0.193096\xi_1 + 0.846011\xi_2)H},\\
N_3(\boldsymbol{\xi}) &= \frac{2.30476}{(1.80194 + 2\xi_1)(-0.781831 - 0.541044\xi_1 + 0.678448\xi_2)H},\\
N_4(\boldsymbol{\xi}) &= \frac{-2.30476}{(1.80194 + 2\xi_1)(0.781831 + 0.541044\xi_1 + 0.678448\xi_2)H},\\
N_5(\boldsymbol{\xi}) &= \frac{1}{(-0.781831 - 0.541044\xi_1 - 0.678448\xi_2)(0.781831 - 0.193096\xi_1 + 0.846011\xi_2)H},\\
N_6(\boldsymbol{\xi}) &= \frac{1}{(0.781831 - 0.781831\xi_1 + 0.37651\xi_2)(-0.781831 + 0.193096\xi_1 - 0.846011\xi_2)H},\\
N_7(\boldsymbol{\xi}) &= \frac{1}{(-0.781831 + 0.781831\xi_1 - 0.37651\xi_2)(0.781831 - 0.781831\xi_1 - 0.37651\xi_2)H},
\end{aligned}
$$

where

$$
H = \frac{7.05418}{AB} + \frac{1.74224}{CD} + \frac{1.74224}{EF} + \frac{3.13941}{BD} - \frac{1.32762}{EG} + \frac{1.32762}{CG} + \frac{3.13941}{AF},
$$

and

$$
\begin{aligned}
A &= 2.07652 - 2.07652\xi_1 - \xi_2,\\
B &= -2.07652 + 2.07652\xi_1 - \xi_2,\\
C &= -1.15238 - 0.797473\xi_1 - \xi_2,\\
D &= 0.924139 - 0.228243\xi_1 + \xi_2,\\
E &= 1.15238 + 0.797473\xi_1 - \xi_2,\\
F &= -0.924139 + 0.228243\xi_1 + \xi_2,\\
G &= 0.704211 + 0.781615\xi_1.
\end{aligned}
$$

A.4. *Octagonal reference element ($n = 8$)*

$$N_i(\boldsymbol{\xi}) = \frac{a_i(\boldsymbol{\xi})}{b(\boldsymbol{\xi})}, \quad (\mathrm{i} = 1, 2, \ldots, 8),$$

where

$$
\begin{aligned}
b(\boldsymbol{\xi}) = 64 \big(&-1 + 5\xi_1^2 - 10\xi_1^4 + 5\xi_2^2 - 20\xi_1^2\xi_2^2 - 10\xi_2^4 +\\
&\sqrt{2}\left(\xi_1^2 + \xi_2^2\right)\left(-3 + 7\xi_1^2 + 7\xi_2^2\right)\big),
\end{aligned}
$$

and

$$
\begin{aligned}
a_1(\boldsymbol{\xi}) &= (-2\xi_1 + A)\,(2\xi_2 + B)\,(-2\xi_1 + C)\,(-2\xi_2 + C)\,(-2\xi_1 + D)\,(-2\xi_2 + D)\,,\\
a_2(\boldsymbol{\xi}) &= (-2\xi_1 + A)\,(2\xi_2 + A)\,(2\xi_2 + B)\,(-2\xi_2 + C)\,(-2\xi_1 + D)\,(-2\xi_2 + D)\,,\\
a_3(\boldsymbol{\xi}) &= (-2\xi_1 + A)\,(-2\xi_1 + B)\,(2\xi_2 + A)\,(2\xi_2 + B)\,(-2\xi_2 + C)\,(-2\xi_1 + D)\,,\\
a_4(\boldsymbol{\xi}) &= -\,(-2\xi_1 + A)\,(-2\xi_1 + B)\,(2\xi_2 + A)\,(-2\xi_1 + C)\,(-2\xi_2 + C)\,(-2\xi_1 + D)\,,\\
a_5(\boldsymbol{\xi}) &= (-2\xi_1 + B)\,(2\xi_2 + A)\,(-2\xi_1 + C)\,(-2\xi_2 + C)\,(-2\xi_1 + D)\,(-2\xi_2 + D)\,,\\
a_6(\boldsymbol{\xi}) &= (-2\xi_1 + B)\,(2\xi_2 + A)\,(2\xi_2 + B)\,(-2\xi_1 + C)\,(-2\xi_2 + C)\,(-2\xi_2 + D)\,,\\
a_7(\boldsymbol{\xi}) &= (-2\xi_1 + A)\,(-2\xi_1 + B)\,(2\xi_2 + A)\,(2\xi_2 + B)\,(-2\xi_1 + C)\,(-2\xi_2 + D)\,,\\
a_8(\boldsymbol{\xi}) &= -\,(-2\xi_1 + A)\,(-2\xi_1 + B)\,(2\xi_2 + B)\,(-2\xi_1 + C)\,(-2\xi_1 + D)\,(-2\xi_2 + D)\,,
\end{aligned}
$$

where

$$
\begin{aligned}
A &= \sqrt{2}\,(-1 + \xi_1 - \xi_2)\,,\\
B &= \sqrt{2}\,(1 + \xi_1 - \xi_2)\,,\\
C &= \sqrt{2}\,(-1 + \xi_1 + \xi_2)\,,\\
D &= \sqrt{2}\,(1 + \xi_1 + \xi_2)\,.
\end{aligned}
$$